

# Simultaneous remote-sensing and in situ observations of plasmaspheric drainage plumes

J. Goldstein<sup>1,5</sup>, B. R. Sandel<sup>2</sup>, M. F. Thomsen<sup>3</sup>, M. Spasojević<sup>4</sup>, P. H. Reiff<sup>5</sup>

## Abstract.

Plasmaspheric drainage plumes are regions of dense plasma that extend outward from the plasmasphere into the outer magnetosphere. We present observations of plumes for two events, 2 June 2001 and 26–27 June 2000. Our observations come from two sources. A global perspective is provided by the IMAGE extreme ultraviolet (EUV) imager, which routinely obtains images of the helium portion of the plasmasphere above total densities of 30–50  $\text{e}^- \text{cm}^{-3}$ . Simultaneous in situ observations of plasmaspheric plumes are obtained by the Magnetospheric Plasma Analyzer (MPA) instruments onboard the Los Alamos National Laboratory (LANL) geosynchronous satellites. The in situ measurements of LANL MPA and the remote-sensing images of IMAGE EUV are complementary data sets that together provide a more complete picture than either alone. The MPA instruments measure density far below the EUV effective density threshold with greater spatial resolution, and often see plasma outside the EUV field of view. Flow speeds are also measurable by MPA. EUV images place the single-point measurements in a global dynamical context and allow separation of spatial and temporal effects. For the 2 June 2001 and 26–27 June 2000 events, both local and global measurements showed the same location, shape and temporal development of the plume(s), and a density distribution obtained from the EUV image at 3:05 UT on 2 June agrees with the LANL MPA density recorded at that time. Analysis of MPA flow data verifies that plume plasma moves sunward, as expected. Sunward flow speeds weaken with decreasing disturbance level, and duskside flow speeds may be increased by the sub-auroral polarization stream. The fine-scale density variations within plumes may be caused by a highly-structured inner magnetospheric E-field, and/or may be existing plasma structure that is carried sunward. The good agreement between the local and global measurements also validates the EUV image mapping method and promises to help quantify EUV images in terms of number density.

## 1. Plasmaspheric Drainage Plumes

The innermost magnetosphere is occupied by the torus of cold dense plasma known as the plasmasphere. From the earliest plasmasphere observations (e.g., *Carpenter* [1967]; *Chappell et al.* [1970a]) and decades of subsequent study, it is known that the plasmopause radial location moves inward during geomagnetic disturbances, a process that came to be known as ‘plasmasphere erosion’ because the inward plasmopause motion was attributed in part to a stripping away of the outer layers of the plasmasphere. Although the details of the plasmasphere erosion process are not en-

tirely understood [*Carpenter and Lemaire*, 1997], one of the known byproducts of erosion is the plasmaspheric drainage plume. Plumes (also called ‘tails’) are regions of (presumably eroded) plasmaspheric plasma, connected to the main body of the plasmasphere, that extend into the more tenuous outer magnetosphere. Plumes were predicted by theoretical models of the disturbance-time inner magnetosphere [*Grebowsky*, 1970; *Chen and Wolf*, 1972; *Spiro et al.*, 1981; *Weiss et al.*, 1997; *Lambour et al.*, 1997] and can be inferred from numerous in situ and ground-based observations [*Chappell et al.*, 1970b; *Horwitz et al.*, 1990; *Carpenter and Anderson*, 1992; *Elphic et al.*, 1996; *Su et al.*, 2001].

Global plasmasphere imaging by the IMAGE satellite extreme ultraviolet (EUV) imager [*Burch*, 2000] has proved the existence of plasmaspheric plumes [*Sandel et al.*, 2001]. The EUV instrument works by detecting 30.4-nm ultraviolet light that is resonantly scattered by the  $\text{He}^+$  ions in the plasmasphere. The existing EUV database contains many examples of plumes during and/or after geomagnetic disturbance times [*Burch et al.*, 2001a, b; *Foster et al.*, 2002; *Goldstein et al.*, 2002, 2003a, c, b; *Sandel et al.*, 2003; *Moldwin et al.*, 2003; *Spasojević et al.*, 2003b, a]. IMAGE EUV provides global snapshots of the plasmasphere and plume with spatial and temporal resolution of about  $0.1 R_E$  and  $\approx 10$  minutes, respectively. The EUV instrument’s effective lower density threshold (i.e., the lowest detectable total plasma density, at which the signal-to-noise ratio is unity) depends

<sup>1</sup> Now at: Space Science and Engineering Division, Southwest Research Institute, San Antonio, TX 78228 USA

<sup>2</sup> Lunar and Planetary Laboratory, University of Arizona, Tucson, AZ 85721 USA

<sup>3</sup> Space and Atmospheric Sciences Group, Los Alamos National Laboratory, Los Alamos, NM 87545 USA

<sup>4</sup> STAR Lab, Electrical Engineering Department, Stanford University, Stanford, CA 94305 USA

<sup>5</sup> Department of Physics and Astronomy, Rice University, Houston, TX 77005 USA

on the intrinsic sensitivity of the instrument as well as the plasma environment being imaged and/or surrounding the imager itself. For intervals of intense geomagnetic activity, the background noise of EUV images is higher than for quieter times, and the effective threshold is then higher, although the intrinsic sensitivity of the instrument is assumed constant. The EUV effective lower threshold has been adequately characterized during quiet or mildly disturbed intervals and is equivalent to about  $30\text{--}50$  electrons $\cdot\text{cm}^{-3}$  [Goldstein *et al.*, 2003c; Moldwin *et al.*, 2003], or  $6\text{--}10$  He $^+$  cm $^{-3}$ , depending on the He $^+$ /H $^+$  ratio. The outer edge of EUV's imaging field of view varies between  $4\text{--}8 R_E$  geocentric distance, with the largest field of view occurring at apogee. Frequently the field of view edge lies at or within geosynchronous orbit.

In situ plasma observations are routinely obtained by the Magnetospheric Plasma Analyzer (MPA) instruments onboard the Los Alamos National Laboratory (LANL) geosynchronous satellites [McComas *et al.*, 1993]. The LANL MPAs measure ion density (presumably predominantly protons) below  $1\text{ cm}^{-3}$  with at least 2–3 times better spatial resolution than EUV. For densities above  $10\text{ cm}^{-3}$  the MPA instruments also obtain in situ flow speeds. The accuracy of the MPA-measured flows is difficult to estimate. There is uncertainty associated with the statistics of the count rate of the instruments, and possible systematic errors associated with asymmetric surface charging, as well as with the energy resolution of the instruments in the range of low-energy ions. Although these effects have not been quantitatively characterized, satellite-to-satellite comparisons and other lines of evidence suggest that the derived MPA flow velocities are probably good to a within factor of 2 when the density is sufficiently high (about  $3\text{ cm}^{-3}$ ). Thus MPA density and flow measurements can provide a local view of plumes that complements the view afforded by EUV images.

In this paper we present simultaneous IMAGE EUV and LANL MPA plume observations for two case studies: a plasmasphere erosion onset on 2 June 2001, and a steady magnetospheric convection (SMC) event on 26–27 June 2000. We show that in these two events, both local and global measurements give the same location, shape, and temporal development of the plume(s). An EUV-derived density distribution from 3:05 UT on 2 June will be shown to agree with simultaneous MPA in situ data. We will include analysis of MPA-measured sunward flow speed inside the plumes, and show that the plume plasma move sunward during disturbances (as expected), and that there is a strong tendency to find high-speed, spatially structured sunward flow regions near dusk, which may be caused by the sub-auroral polarization stream [Foster and Burke, 2002], and which are apparently connected to fine-scale density variations within plumes.

## 2. Erosion Onset: 2 June 2001

### 2.1. Brief Overview

Between 0–6 UT on 2 June 2001, EUV observed an erosion of the plasmasphere in which the nightside plasmopause moved inward by approximately  $2 R_E$ , and the dayside plasmopause moved sunward to form a broad plume that extended beyond the field of view of EUV's cameras and which narrowed in local time as the event progressed. The erosion was apparently triggered by a southward IMF transition. Figure 1 contains measurements of the MAG [Smith *et al.*, 1998] and SWEPAM [McComas *et al.*, 1998] instruments on

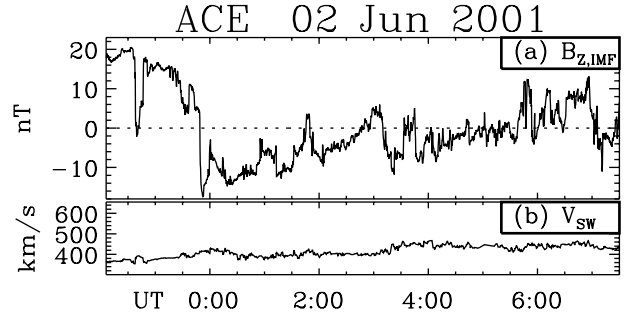


**Figure 1.** Measurements of the ACE MAG and SWEPAM instruments on 2 June 2001 during the first part of the day. (a) IMF north/south polarity, (b) solar wind speed. The southward IMF turning at 23:49 UT triggered plasmaspheric erosion.

the ACE spacecraft, which on 2 June was about  $226 R_E$  (or about 55 minutes) upstream from a nominal  $10 R_E$  magnetopause. Panel (a) plots the  $Z$ -component of the IMF, and panel (b) shows the solar wind speed  $V_{sw}$ ; both have been delayed to account for propagation to the magnetopause. The abrupt change to southward IMF at 23:49 UT on 1 June presumably led to enhanced sunward flows which eroded the plasmasphere starting at about 00:21 UT on 2 June [Goldstein *et al.*, 2003b].

### 2.2. Global Images and In-Situ Density at Geosynchronous Orbit

The top row of Figure 2 shows four snapshot EUV images taken during the 2 June erosion event. In raw EUV images (not shown) the brightness of each pixel is proportional to the number of 30.4-nm photons accumulated from along the line of sight, per 10 minutes (5 spins of the IMAGE satellite). Each raw pixel-vertex has been mapped to the equator by assigning to each point the minimum dipole  $L$ -shell along the line of sight [Roelof and Skinner, 2000; Goldstein *et al.*, 2003c]. This mapped signal image is then converted to column abundance using estimates for the rate of resonant scattering and the solar flux at 30.4-nm (the latter based on the Solar2000 solar flux model of Tobiska *et al.* [2000]). Thus, in each panel of the top row, the color scale gives an equatorial distribution (versus radius  $L$  and magnetic local time MLT) of line-of-sight-integrated column abundance in He $^+$  cm $^{-2}$ . In each panel of the bottom row of Figure 2 is a plot of points (the blue circles) that have been manually extracted from the EUV image directly above the plot. These extracted points do not necessarily follow a single contour of brightness; they are intended to highlight certain components of the EUV images. In the following discussion, we will refer to features visible in the images (top row) of Figure 2, but these features are also labeled and identified in the plots of extracted points (bottom row) for the reader who is not familiar with interpretation of EUV images.

In Figure 2(a) the plasmasphere extends out to large radial distances, with no clear plasmopause and irregular azimuthal density structure. Outlying plasma with density close to the EUV lower threshold shows up as speckling near the field-of-view edges. Speckling throughout the image is suggestive of fine-scale structure that is unresolved by EUV imaging. However some of the speckling, especially at large  $L$ , is undoubtedly due to background noise, and the bright

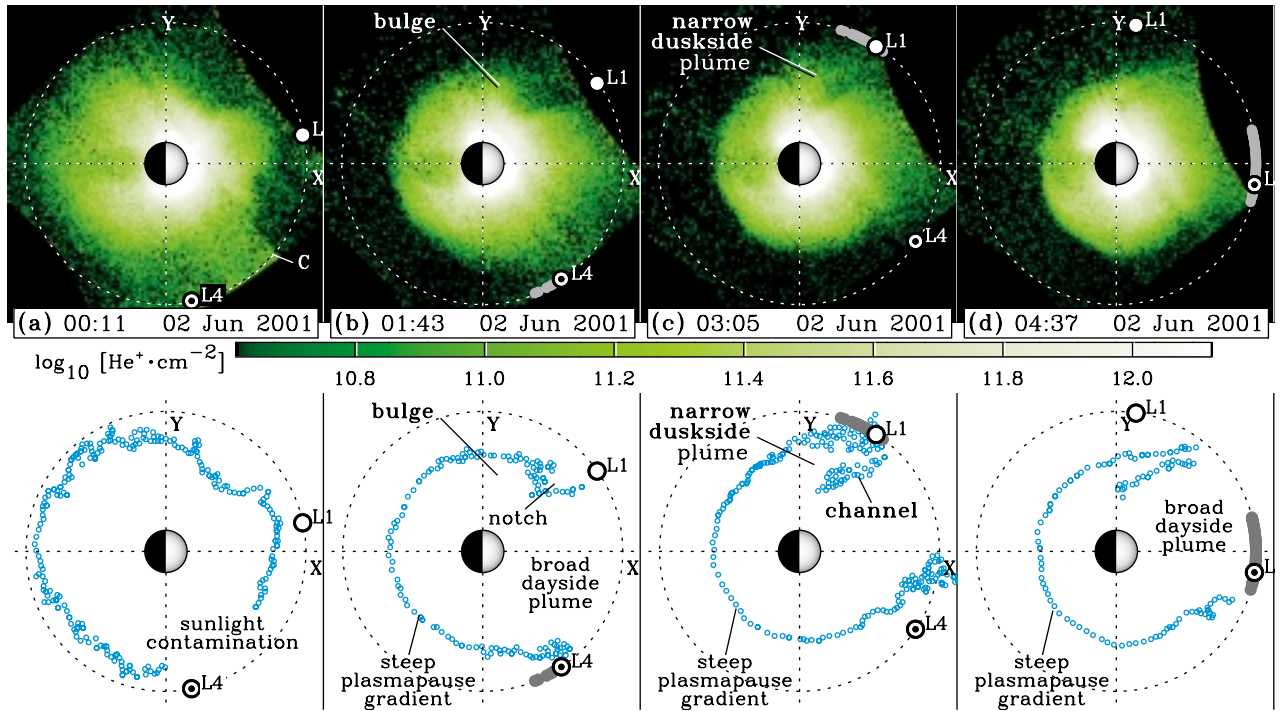


**Figure 2.** *Top row:* The onset of the 2 June 2001 plasmaspheric erosion as seen by IMAGE EUV and LANL MPA, at the times/dates given at the bottom of each panel. The color intensity is EUV equatorial  $\text{He}^+$  abundance, as given by the scale at the bottom of the plot. The Earth is at the center of each plot; dotted lines indicate the X- and Y-axes (SM coordinates) and geosynchronous orbit. The black triangular regions in the corners of each plot mark the EUV field-of-view edges. The bright patch ‘C’ in 2(a) is sunlight contamination. The gray highlighted sections of geosynchronous orbit indicate where LANL satellites 1991-080 (‘L1’, the white dot) and 1994-084 (‘L4’, the bull’s-eye) saw plasmaspheric plasma. (See Figure 3.) Observations by EUV and MPA agree that the 2 June erosion onset was marked by a sunward surge of plasma, creating a broad dayside plume.

*Bottom row:* In each panel, the blue circles are manually-extracted points from the EUV image above it, highlighting the features discussed in the text. The positions of the LANL satellites and intervals of MPA-observed plasmaspheric plasma are indicated in same format as the top panels.

area labeled ‘C’ in the post-dawn MLT sector, just inside the field-of-view edge, is sunlight contamination. Following the erosion onset, as shown in 2(b), 2(c) and 2(d), the night-side plasmopause moved inward and achieved a steep, well-defined gradient. Exterior to this plasmopause gradient, the outlying low-density plasma of 2(a) was removed by the erosion, as is evident from the dark background. The dayside plasma moved sunward, forming a broad plume in the morning and afternoon MLT quadrants. A bulge of plasma can be seen in Figure 2(b), at  $L = 4-5$ , just west of 18 MLT. West of the bulge is a ‘notch’ centered at  $\approx 15$  MLT, where the plasmopause radius is reduced relative to the surrounding MLT. Panels 2(c) and 2(d) show that during the erosion, the bulge of 2(b) was elongated into a narrow duskside plume that extended sunward outside the EUV field of view, separated from the main dayside plume by a narrow, hazy, low-density channel, which is the remnant of the notch of 2(b), is almost undetectable in 2(d). In the images, both the thin duskside plume and the main dayside plume become more tenuous (i.e., darker in color) with increasing radial distance. This is consonant with the convection interpretation that the material in the plume is moving to larger radial distances where larger flux tube volumes (and thus lower densities) are found.

Figure 3 shows ion density data obtained on 2 June 2001 by the Magnetospheric Plasma Analyzer (MPA) instruments [McComas *et al.*, 1993] onboard the Los Alamos National Laboratory (LANL) geosynchronous satellites ‘L1’ (1991-

080) and ‘L4’ (1994-084). Following *Elphic et al.* [1996], trajectories of L1 and L4 are plotted in MLT versus UT as dotted lines, and the MPA-measured ion densities (in  $\text{cm}^{-3}$ ) are superimposed on the satellite trajectories with the vertical scale 2 MLT hour =  $40 \text{ cm}^{-3}$ , as indicated in the legend. For reference, a dot-dash line parallel to the LANL trajectories indicates  $40 \text{ H}^+ \text{ cm}^{-3}$ .

In discussing the dynamics that produced the geosynchronous density profiles, it is informative to compare the in situ LANL data of Figure 3 to the global images of Figure 2. For reference, the times of the four EUV snapshots in Figures 2(a)–(d) are indicated by the vertical dashed lines in Figure 3. Also, in Figure 2 portions of the geosynchronous orbit have been highlighted in gray to indicate where the LANL satellites observed plasmaspheric plasma regions, and the locations of L1 and L4 are plotted in each panel. At time (a), 00:11 UT, both L1 and L4 were outside the plasmasphere and observed densities below about  $4 \text{ H}^+ \text{ cm}^{-3}$ . This is consistent with the faint green speckling (which generally indicates densities at or below the EUV noise floor) at the very outer edges of the EUV image of Figure 2(a), except in the post-dawn MLT sector (in the vicinity of L4) where sunlight contamination creates an artificially bright region in the image.

First the L1 data during the erosion will be discussed. Plasmaspheric erosion commenced at 00:21 UT, according to EUV observations (not shown). During the earliest phase

of the erosion, L1 was located inside the 15 MLT ‘notch’ (mentioned above) and so continued to observe low density. As the erosion proceeded, the sunward surging plasma began to fill up the notch, as reflected by the L1 density profile between vertical lines (b) and (c) in Figure 3.

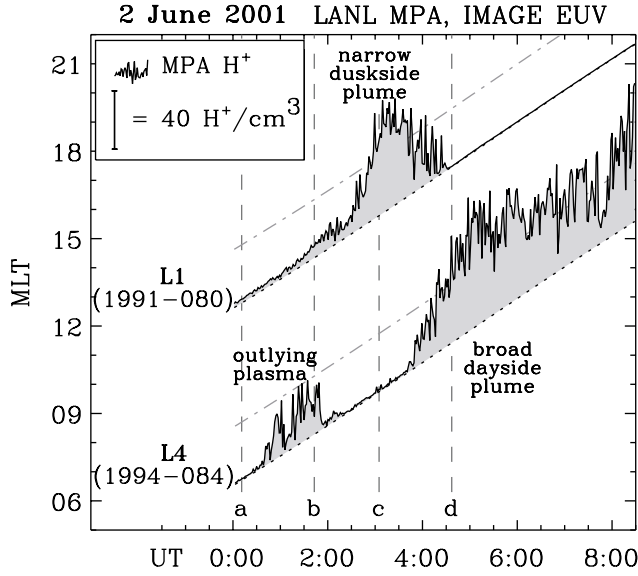


**Figure 3.** LANL MPA measurements showing three intervals of plasmaspheric plasma on 2 June 2001, plotted along the UT–MLT trajectories of two LANL satellites. The times of the four snapshots from Figure 2(a), (b), (c), (d) are indicated by the vertical dashed lines. The single L1-observed plasmaspheric plasma region arose from a narrow duskside plume that elongated past geosynchronous orbit at about 3 UT. L4 observed low-density outlying plasma that was swept sunward past the satellite at about 2 UT. Just before 4 UT, L4 rotated into an existing broad dayside plume that began rotating with the satellite after quieting at about 6 UT.

The increase in L1 density just before (c) 03:05 UT occurred as the bulge of Figure 2(b) was elongated into the narrow duskside plume that crossed geosynchronous orbit in Figure 2(c). The gray highlighted portion of the L1 orbit in Figure 2(c) shows the portion of the L1 profile above the EUV threshold ( $40 \text{ H}^+ \text{ cm}^{-3}$ ); this orbit segment matches nicely with the EUV observations of the narrow duskside plume. After (d) 04:37 UT L1 had crossed the dusk edge of the plume and exited to the low-density outer magnetosphere. In Figure 3 the L1 plume density between (c) 03:05 UT and (d) 04:37 UT is quite close to the average EUV threshold ( $40 \text{ H}^+ \text{ cm}^{-3}$ ), consistent with the very faint signal intensity surrounding L1 in Figure 2(c).

The L4 profile exhibits two intervals of plasmaspheric plasma, between (a)–(b) and starting just before (d). Shortly after the erosion commenced, L4 began rotating into an outlying plasma region at or below the EUV threshold, with density between  $5 \text{ H}^+ \text{ cm}^{-3}$  and  $40 \text{ H}^+ \text{ cm}^{-3}$ . This plasmaspheric plasma in the L4 profile between (a)–(b) is highlighted in gray in Figure 2(b). The EUV images of Figures 2(b) and 2(c) put the L4 (a)–(b) plasmaspheric plasma into a global dynamical context. Shortly after L4 rotated into this outlying plasma, as shown in Figure 2(b), the outlying plasma was convected sunward past L4, so that after (b) 01:43 UT, L4 observed density below  $5 \text{ H}^+ \text{ cm}^{-3}$ , consistent with the black region surrounding L4 in Figure 2(c). Interpretation of the L4 plasmaspheric plasma density seen during (a)–(b) is ambiguous because it lies mostly well below the EUV threshold. The dim speckling surrounding L4 in Figure 2(b) is suggestive of a low-density dawnside portion of the broad dayside plume, but this interpretation is complicated by the fact that this sector of the EUV image suffered mild sunlight contamination. It is also possible that the (a)–(b) plasmaspheric plasma is an isolated blob, which could arise in at least two ways. First, a highly structured flow field might cause a blob of plasmaspheric plasma to detach from the nightside plume. Second, a highly-structured region of plume plasma could move outward in  $L$ , and as it does so, the average plume density would decrease as the flux tube volume increased. The original plume

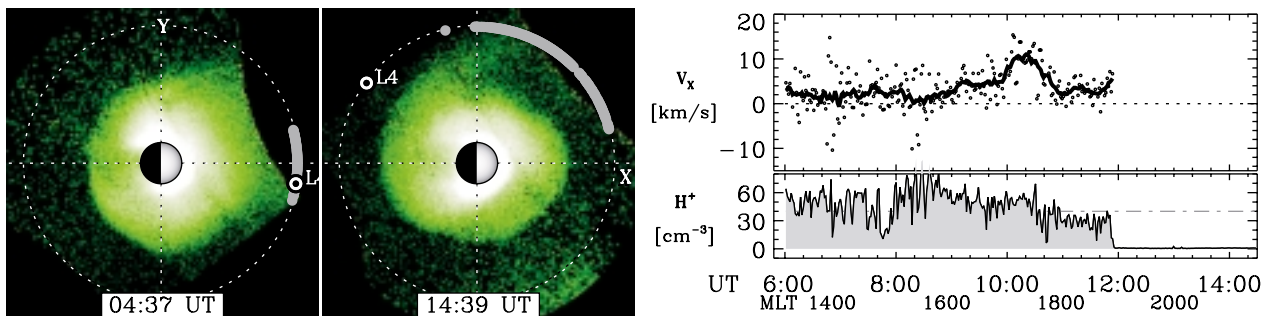


**Figure 4.** Evidence of plume wrapping, 2 June 2001 seen by IMAGE EUV and LANL MPA. *LEFT:* The leftmost panel reproduces the 4:37 UT EUV image of Figure 2(d), with the L4  $\text{H}^+$  density above  $40 \text{ H}^+ \text{ cm}^{-3}$  and before 6 UT highlighted in gray. At 4:37 UT, EUV saw a broad dayside plume, and LANL satellite L4 had recently crossed the western edge of this plume. *MIDDLE:* The middle panel shows the EUV image from 14:39 UT. A northward IMF turning at  $\sim 6$  UT presumably reduced the convection strength, causing the plume to begin rotating eastward and wrapping about the plasmasphere. At 14:39 the duskside edge of the plume was at about 18–19 MLT. The gray highlighted sections of geosynchronous orbit show L4 plasmaspheric plasma above  $40 \text{ H}^+ \text{ cm}^{-3}$  and after 6 UT. The LANL MPA plume location agrees with that of EUV. *RIGHT:* The right panels show LANL MPA density and flow data after 6 UT recorded by L4, which crossed the duskside edge of the plume at 19 MLT, but the density fell below the EUV threshold at  $\sim 18$  MLT. The flow data show that the dayside plume plasma was moving sunward at 2–4 km/s, but near the duskside edge, sunward flows increased to  $\sim 10$  km/s.

structure, which initially sat atop a large average density, would eventually produce isolated density structures as the plume moved outward and became more tenuous. The large amount of structure within the L4 (a)–(b) plasmaspheric plasma is consistent with both of these blob-formation scenarios. Regardless of the spatial form of this L4-observed plasma (either an isolated blob or low-density plasma connected to the dawnside portion of the dayside plume), the MPA flow data (discussed in the next subsection) support the interpretation that the plasma was convected sunward past the L4 satellite.

After (b) 01:43 UT, the broad dayside plume created by the sunward surge gradually narrowed in MLT as the western edge of the plume moved eastward; during this time L4 gradually caught up to the eastward-moving western edge, and crossed it at about 4 UT, as can be seen (in Figure 3) by the large increase in the  $H^+$  density profile at that time. In Figure 2(d) L4 can be seen just inside the western edge of the plume, and just at the EUV field-of-view edge (i.e., the black region that cuts across the broad dayside plume in the post-noon MLT sector). After (d) 04:37 UT the EUV images provide no more information about the dayside plume at geosynchronous orbit, but the L4  $H^+$  densities are clearly that of plume plasma; the portion of this plume above  $40 H^+ \text{cm}^{-3}$  and before 6 UT is highlighted in gray in Figure 2(d). We note that L4 observed plume plasma well beyond 6 UT, and did not cross the eastern edge of this plume until 12 UT, at 19 MLT, as shown in the bottom right panel of Figure 4. These later L4 observations indicate that once the erosion event had ceased (after the northward IMF turning at about 6 UT; see Figure 1), the plume began rotating eastward and wrapping around the plasmasphere. This plume wrapping process was predicted by *Grebowsky* [1970] to occur when the corotation-dominated region expands (during quieting) to include the plume which extended into the convection-dominated region during the erosion. A radial shear in the corotational flow speed causes the outer edge of the plume to move eastward more slowly than the inner edge, causing the plume to become wrapped around the plasmasphere. In models (e.g., *Grebowsky* [1970] and others cited in the introduction), the wrapping plume’s eastern edge rotates eastward until it encounters the newly-expanded boundary between closed (corotational) and open (convectonal) drift paths. Plume wrapping in global EUV images has been reported by *Spasojević et al.* [2003b]. There are no EUV observations of the plume rotation between 6–12 UT, but the next available EUV images at 12:18–19:38 UT show evidence of a rotated, wrapping plume whose eastern edge is at approximately 19 MLT, entirely consistent with the LANL data. Although the EUV coverage begins at 12:18, the first image with a field of view that encompasses geosynchronous orbit is at 14:39 UT, shown in the middle panel of Figure 4. The L4 plasmaspheric plasma density above  $40 H^+ \text{cm}^{-3}$  is indicated by the gray orbit segments overlaid on the EUV images, and is broken up into two time intervals as follows. In the leftmost panel of Figure 4 the gray highlight indicates L4 plasmaspheric plasma before 6 UT (i.e., while the erosion was still occurring), and in the middle panel the gray indicates L4 plasmaspheric plasma after 6 UT (i.e., once the plume presumably began rotating and wrapping after the northward IMF turning). The EUV images of Figure 4 depict global dynamic change/reconfiguration of the plasmasphere that occurred between 4:37 and 14:39 UT. The rise in L4 density before (d) happened when the satellite crossed

the eastward-moving western plume boundary (as discussed above). Following the 4:37 UT image, we suggest a hypothetical sequence of events consistent with available data and expected plasmasphere behavior (based on the models mentioned above and in the introduction), as follows. At some time (which we speculate is 6 UT when the IMF turned northward) the plume began rotating eastward, and the L4 trajectory was such that it remained within the eastward-moving plume and continued to see plasmaspheric plasma. When the plume’s eastern edge encountered the corotation-convection boundary located at about 19 MLT, the plume ceased rotating (but continued wrapping inside the convection zone). At 12 UT (and 19 MLT), L4 crossed the eastern edge of this wrapping plume. As shown by the L4 plasmaspheric plasma overlaid on the EUV image of Figure 4, there is good agreement between this L4-observed eastern edge at (12 UT, 19 MLT) and the 18–19 MLT location of the dusk edge of the plume in the 14:39 UT EUV image. Assuming our hypothetical event sequence is correct, this good agreement suggests that the eastern/dusk side edge of the wrapping plume did not move in the time between 12 UT and 14:39 UT, consistent with a roughly stationary corotation-convection boundary.

### 2.3. Flow at Geosynchronous Orbit

Although the EUV images suggest that plasma moves sunward inside the dayside plumes, it is difficult to verify this directly from EUV images alone. However, flows inside plumes can be measured by the LANL MPA instruments [*Borovsky et al.*, 1998; *Thomsen et al.*, 1998]. Figure 5 depicts flows measured by the L1 and L4 satellites during the 2 June erosion onset. The top two panels 5(a) and 5(b)

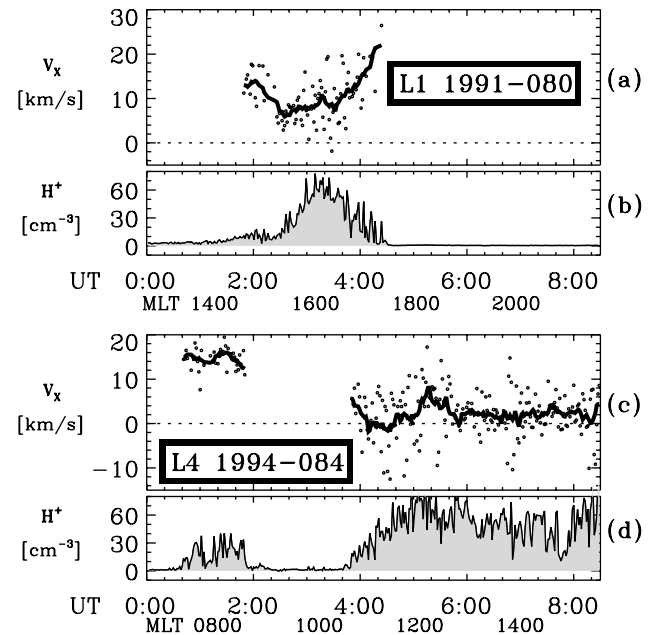


**Figure 5.** LANL MPA sunward flows seen on 2 June 2001 during the plasmasphere erosion. Panels (a) and (c) plot the  $X$ -component of the flow speed (in km/s) for L1 and L4 respectively. Flows are plotted in the inertial frame. The bold curves are the 14-minute averaged sunward flows. Panels (b) and (d) contain  $H^+$  number density (in  $\text{cm}^{-3}$ ) for L1 and L4. On average, plume plasma moves sunward ( $V_x > 0$ ).

show sunward flow speed and density for L1; the bottom two panels 5(c) and 5(d) plot L4 data. Only flows inside plasmaspheric plasma (i.e., for density above  $10 \text{ H}^+ \text{ cm}^{-3}$ ) are shown. The raw flow data (plotted as dots) fluctuate quite a bit, on roughly the same scale size as the density structure, possibly indicating that the fine-scale density structure is related to spatial variation in the flow (or electric) field of the inner magnetosphere, as was suggested by *Moldwin et al.* [1995]. Another possibility is that these fluctuations are in some way related to the uncertainty in the flow-speed measurements made by the MPA instruments, which is difficult to quantify, as mentioned in the introduction. We shall limit the following discussion to 14-minute boxcar averages of the flow data, which smooth out these fluctuations, whatever their cause.

The general trend, as given by the 14-minute averaged curves (plotted as bold lines) is that plume plasma moves sunward ( $V_X > 0$ ). At geosynchronous orbit, a 0.1 mV/m electric ( $E$ ) field would cause cold plasma (in a dipole magnetic field) to  $E \times B$ -drift at about 1 km/s. Therefore, the sunward flow speeds recorded by L1 and L4 before about 4:00 may correspond to  $E$ -field strengths of  $\approx 1$  mV/m or more. In the overlap region of L1 and L4 coverage (Figure 5), the flow velocity at L1 (predusk) is simultaneously much greater than that at L4 (in the prenoon sector). This differs from standard convection models, which predict a stagnation point in the dusk region (where corotation cancels convection), and faster flows on the dawnside (where corotation adds to convection). Some of these strong sunward flow speeds seen inside the narrow duskside plume (L1 from 2–4 UT) may be due to the sub-auroral polarization stream (SAPS) [*Goldstein et al.*, 2003b], an intense narrow flow channel that arises during disturbance times as a consequence of ring-current/ionosphere coupling [*Foster and Burke*, 2002]. Note the flow speed in this L1 narrow duskside plume increases toward dusk, consistent with a SAPS interpretation. The strong sunward flow ( $> 10$  km/s) inside the outlying L4 plasma before 2:00 occurs when the IMF is most strongly southward, and so can be attributed to strong dawnside convection. Later in the erosion event, the sunward flows seen by L4 on the dayside, inside the plume, are much slower. This may be related to the fact that after 4:00 UT the IMF was only weakly southward, presumably leading to reduced convection flow strength. Slower (2–4 km/s) sunward flow speeds continued to be recorded by L4 from 6–10 UT (shown in the top right panel of Figure 4, and then the sunward flow speed increased to about 10 km/s as L4 approached the eastern edge of the rotated wrapping plume. These 10 km/s flows may also be related to SAPS activity. Overall, the LANL MPA flow data of 2 June 2000 support the interpretation that plumes arise as dense plasma is stripped away from the plasmasphere and convects sunward, as predicted by theoretical models (see also *Borovsky et al.* [1998]; *Thomsen et al.* [1998]).

#### 2.4. EUV Number Density

The mapped EUV images of Figure 2 can in principle be converted to an equatorial  $\text{He}^+$  number density with some assumptions for the field-aligned and radial density profile. In this section we obtain a number density distribution that is roughly consistent with LANL MPA in situ observations. We sought only to get an order-of-magnitude estimate, and used the following assumptions. We took the density to be

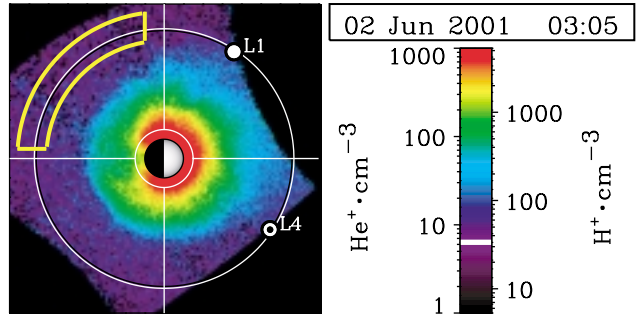


**Figure 6.** Ion number densities produced from the EUV mapped image of Figure 2(c). The line-of-sight  $\text{He}^+$  column abundance has been crudely converted into an equatorial  $\text{He}^+$  number density, as given by the left side of the colorbar scale next to the plot. The ratio  $\text{He}^+/\text{H}^+ \approx 0.19$  yields the  $\text{H}^+$  number density scale indicated on the right side of the colorbar. Note that the narrow duskside density channel visible in Figure 2(c) is still present in this distribution, but it is difficult to see with the colorbar chosen to display the density. The innermost (i.e., closest to the Earth) extent of the hazy low-density channel shows up in the density distribution as a ‘notch’-like feature at  $\sim 17$  MLT in the 300–1000  $\text{H}^+ \text{ cm}^{-3}$  (green color) range.

constant along magnetic field lines, and assumed the radial dependence inside the plasmasphere to be that of *Carpenter and Anderson* [1992]. The radial/field-aligned dependence needs to be specified in order to determine the path-length of the line of sight of each EUV pixel. The results are fairly insensitive to the choice of radial profile, and a comparable density can be obtained using, for example, a much steeper  $1/L^4$  radial dependence. For simplicity, we assumed an EUV line of sight normal to the magnetic equator (i.e., parallel to the magnetic pole axis); again, the result is quite insensitive to small tilts of the line of sight with respect to the magnetic axis. The result is shown in Figure 6.

Figure 6 contains a plot of the  $\text{He}^+$  density distribution in the magnetic equator. The colorbar at the right of the plot gives the density scale (in  $\text{He}^+ \text{ cm}^{-3}$ ) associated with the color table; the colorbar is saturated at  $1000 \text{ He}^+ \text{ cm}^{-3}$ . Because the low-altitude ( $L < 1.5$ ) dayside EUV signal contains significant contributions from dayglow, densities in this region are less certain. Also, although there is very likely a real day/night asymmetry in the high-density (red) inner plasmasphere, some of the observed asymmetry is due to a reduction in the 30.4-nm emission in the Earth’s shadow.

There is a steep nightside plasmopause gradient in which the density drops from about  $80 \text{ He}^+ \text{ cm}^{-3}$  (border between green and light blue) to  $8\text{--}10 \text{ He}^+ \text{ cm}^{-3}$  (indigo/dark-blue border) in about  $1 R_E$ . Just outside the nightside plasmopause the distribution flattens out to a slightly noisy indigo background in Figure 6. This relatively flat background is found in regions in which the plasma number density is below the EUV instrument lower threshold. Thus, the indigo background is the ‘noise floor’ of EUV; the apparent emptiness of the indigo background region does not mean that there is no low-density plasma outside the plasmopause. The average EUV lower threshold is known (in terms of total electron density) to be  $40 \text{ e}^- \text{ cm}^{-3}$  [*Goldstein et al.*, 2003c]. If we determine the lower threshold (in terms of  $\text{He}^+$  density) from the density distribution of Figure 6, we can estimate

the plasmaspheric  $\text{He}^+/\text{H}^+$  ratio. The noise floor is physically meaningful (in terms of a density value) only where plasma gradients cross the noise floor; however, it is easiest to measure the density value of the (relatively flat) noise floor at locations far from plasma gradients. The annular section in the premidnight quadrant (enclosed by the bold yellow lines) contains only counts that are representative of the noise floor. The average value in this annular section (and thus the  $\text{He}^+$  density value of the EUV noise floor, i.e., an upper limit on the density of plasma in this region) is  $6.3 \text{ He}^+ \text{ cm}^{-3}$ ; this value is indicated in the colorbar with a horizontal white line segment. Assuming correspondence with the average EUV lower threshold of  $40 \text{ e}^- \text{ cm}^{-3}$  yields a helium to electron ratio of  $6.3/40 \approx 0.16$ . This implies the proton to electron ratio is about 0.84. From this we find  $\text{He}^+/\text{H}^+ \approx 0.19$ , a reasonable value [Comfort *et al.*, 1988; Craven *et al.*, 1997].

Using this derived ratio, the colorbar in the plot can also be scaled to  $\text{H}^+ \text{ cm}^{-3}$ , and we can directly relate the EUV-derived density distribution to MPA  $\text{H}^+$  density. The  $\text{H}^+$  densities in the equatorial distribution of Figure 6 are reasonable in terms of average plasmaspheric density distributions, and by inspection are roughly consistent with LANL MPA data. For example, at the 3:05 UT location of L1 in the figure, the EUV  $\text{H}^+$  number density is about  $60 \pm 30 \text{ cm}^{-3}$ , where the large uncertainty includes both the noisiness of the EUV image near the L1 location in Figure 6 and also the many assumptions required to obtain the EUV density estimate. Taking into consideration the crudeness of the EUV abundance/density conversion, this EUV density agrees surprisingly well with the L1 density  $50 \pm 5 \text{ cm}^{-3}$  measured at (c) 3:05 in Figure 3. A similar comparison by Dent *et al.* [2003] between EUV images and in situ density measured by the IMAGE radio plasma imager (RPI) [Reinisch *et al.*, 2001] yielded good qualitative agreement, but the  $\text{He}^+/\text{H}^+$  ratio they obtained was about 8 times smaller than the nominal range 0.1–0.2. One explanation for our higher  $\text{He}^+/\text{H}^+$  ratio is that we used an updated version of the Tobiska *et al.* [2000] Solar2000 30.4-nm solar flux model [Tobiska, private communication, 2003].

Ideally, we would perform a more detailed quantitative comparison by flying virtual LANL satellites through a time-sequence of EUV-derived density distributions. However, for the 2 June 2001 event we found that there were only very brief (10–30 minute) intervals where either satellite (L1 or

L4) was in place to record dense plasmaspheric plasma that was in the EUV field of view and above the EUV threshold; the 3:05 UT snapshot is within one such interval. (For the second case study 26–27 June 2000 of the next section, we also found only brief intervals with LANL satellites simultaneously inside the plasmasphere and the EUV field of view. Therefore, we did not perform a detailed point-by-point EUV-MPA comparison for the second event either.) To avoid this difficulty in future EUV-MPA comparisons, we plan to identify extended quiet periods of ionospheric filling, such that dense ( $>30\text{--}40 \text{ H}^+ \text{ cm}^{-3}$ ) plasmaspheric plasma is found at geosynchronous orbit for long periods of time. Such a strategy would increase the probability that the LANL satellites are simultaneously in the EUV field of view and also observing dense plasmaspheric plasma, and possibly aid in producing more refined conversion of EUV images to number density distributions.

### 3. Plume Evolution: 26–27 June 2000

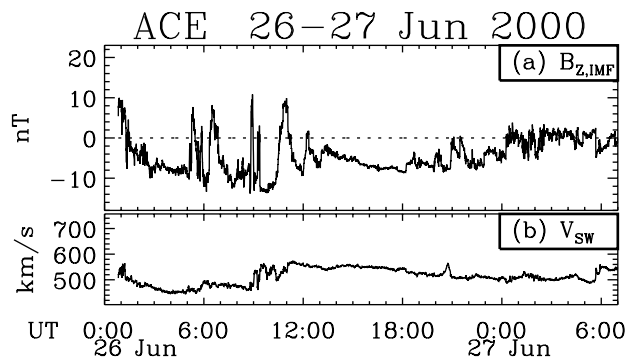
#### 3.1. Brief Overview

Figure 7 shows measurements of the ACE spacecraft, plotted in the same format as Figure 1. The two panels are (a) the Z-component of the IMF and (b) the solar wind speed  $V_{\text{sw}}$ , both time-propagated to the magnetopause. The ACE measurements show that the IMF turned southward early on 26 June, following quiet conditions that prevailed for most of the previous day. Before about 13 UT the IMF on 26 June exhibited several abrupt polarity transitions between strong southward ( $-8 \text{ nT}$  to  $-13 \text{ nT}$ ) and moderate-to-strong northward ( $4 \text{ nT}$  to  $9 \text{ nT}$ ). During the period 13–20 UT the IMF and solar wind speed were relatively stable, and a ‘steady magnetospheric convection’ (SMC) condition prevailed [Yahnin *et al.*, 1994; E. Sanchez, private communication, 2002].

#### 3.2. Global Images and In-Situ Density at Geosynchronous Orbit

The EUV observations of this event are presented in Figure 8 (following the format of the top row of Figure 2). The positions of LANL satellites 1991-080 (‘L1’), 1994-084 (‘L4’) and 1989-046 (‘L9’) are given by the white dot, bull’s-eye and triangle, respectively. Gray-highlighted sections of geosynchronous orbit represent intervals where plasmaspheric plasma was observed. The LANL measurements of 26 June and 27 June 2000 are shown in Figure 9 and Figure 10 (respectively), in the same format as Figure 3.

No EUV measurements were available during the first 11 hours of 26 June, but the LANL observations indicate an initially mild sunward surge that created a narrow afternoon-sector plume (seen by L9 between 4–5 UT in Figure 9). By 6 UT this narrow plume had expanded to fill the afternoon sector between 12–15 MLT with  $30\text{--}80 \text{ H}^+/\text{cm}^{-3}$  plasma (seen by L4 between 5:30–7:30 UT in Figure 9). The L4 observations after 7:30 UT indicate a  $<30 \text{ cm}^{-3}$  plasma distributed between 15–17 MLT in Figure 9. The LANL MPA density data contain a great deal of spatial structure in the surging plume. Possible explanations for this fine structure include: (1) a spatially-structured and/or rapidly-varying inner magnetospheric flow field, and/or (2) preservation of fine structure originally found in the quiet-time plasmasphere, which is then carried sunward during the erosion. A highly structured flow field (1) can be related to unsteady



**Figure 7.** ACE measurements on 26–27 June 2000, in the same format as Figure 1. During the steady magnetospheric convection (SMC) that transpired between 13–20 UT on 26 June, the plasmasphere was eroded and a dayside plume formed.

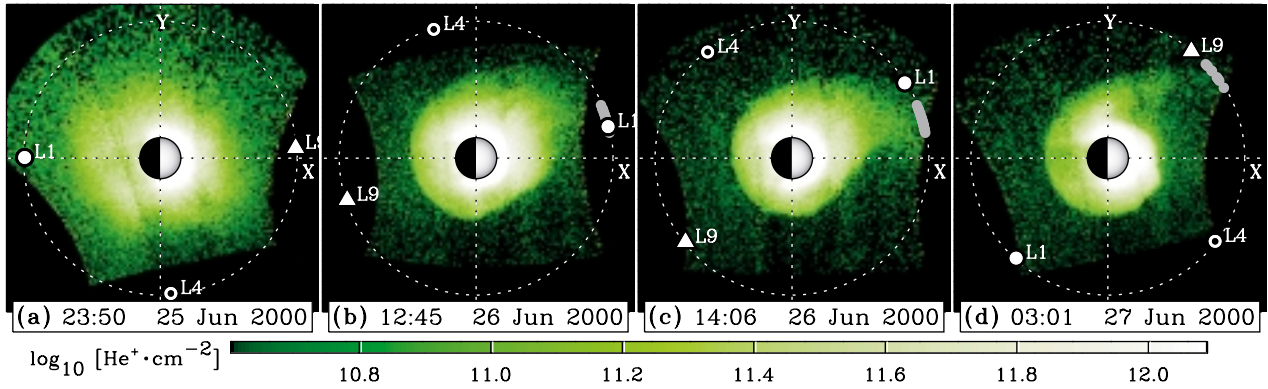


**Figure 8.** Four snapshots of the plasmasphere depicting the 26–27 June 2000 SMC event, in the same format as the top row of Figure 2. Observations (EUV and MPA) indicate that the erosion caused a dayside plume (panels (b), (c)) that narrowed over the course of several hours and then began rotating/wrapping during quieting (panel (d)).

southward IMF in the early part of the day, or perhaps flow-shear instabilities in the fast (presumably SAPS) flow channels [Borovsky, private communication, 2003]. Explanation (2) is plausible because of the irregularly-shaped, spatially-structured plasmasphere seen in the quiet-time image of Figure 8(a).

After 11 UT on 26 June the EUV images and LANL MPA data provide concurrent observations of the development of the plume. In Figure 8(b) the 12:45 UT EUV image contains a smooth, eroded nightside plasmopause. A dayside plume extends sunward from the main plasmasphere between 13–15 MLT. L1 entered the western (13 MLT) edge of this plume at 12:45, as shown by the gray highlighted orbit segment in Figure 8 and the plasmaspheric plasma region between 12:45–14:06 (dashed vertical lines (b)–(c)) in Figure 9. The 13 MLT western edge of the plume, observed at 12:45 UT, (Figure 8(b)) was roughly 1 MLT-hour eastward of its observed position seven hours earlier (6 UT) as seen by L4 in Figure 9, indicating the plume had narrowed in MLT. The plume continued to narrow in the sequence of EUV images following panel 8(b).

At the time of the next EUV snapshot in Figure 8(c), the eastern edge of the plume had moved 1 MLT hour westward

to 14 MLT. We speculate that this westward motion of the dusk plume edge happened in response to an intensification of sunward flow at the dusk side plasmopause. LANL satellite L1 crossed the location where EUV saw the 14 MLT edge before 13:30 UT. At that time, L1 was in a very structured region of declining density (Figure 9), suggestive of the diffuse dusk plume edge in EUV data. However, L1 experienced a data gap shortly afterward, so there may have been more plasma (perhaps below EUV’s threshold) beyond that point. It is worth mentioning that although the L1 plume densities are somewhat below the nominal/statistical EUV lower threshold of  $40 \text{ H}^+ \text{ cm}^{-3}$ , the EUV image intensity at geosynchronous orbit is still noticeably above the black background in panel (c); the EUV effective lower threshold may have been slightly lower than average (perhaps due to higher 30.4-nm solar flux or above-average  $\text{He}^+$  concentration). In Figure 8(d) the EUV plume density near geosynchronous orbit falls mostly below the instrument lower threshold (i.e., noise floor). However, the MPA-observed plume is clearly visible in the L9 profile (Figure 10) before 3 UT. Comparison between the EUV image of Figure 8(d) and the superimposed L9 plasmaspheric plasma region (gray segment) shows that the distinctness of the plume structure extends

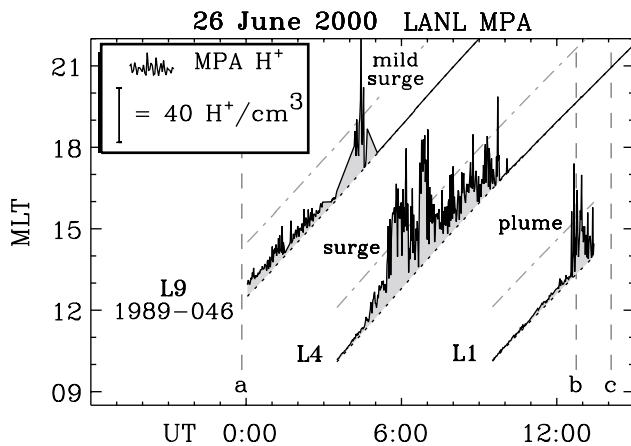


**Figure 9.** 26 June 2000 LANL MPA observations showing the initial sunward surge and plume formation (seen by L9 and L4 before 12 UT), and the EUV-observed plume of Figure 8 (seen by L1 after 12 UT).

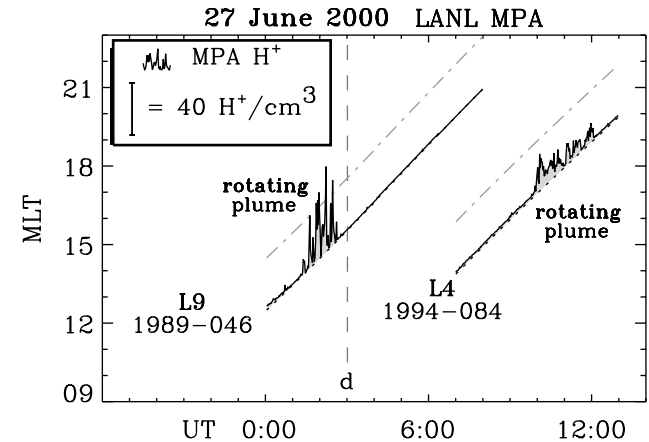


**Figure 10.** 27 June 2000 LANL MPA observations showing the plume rotating eastward (i.e., to later MLT) after the cessation of southward IMF. The plasmaspheric plasma seen by L9 is the geosynchronous signature of the EUV-observed plume at (d) 3:01 UT in Figure 8.

to geosynchronous orbit at least, even though the geosynchronous plume signature is very faint in the EUV image. This in turn implies that the flows responsible for the plume extend at least to geosynchronous orbit.

As shown in Figure 7 very weak northward IMF was observed during the first six hours of 27 June. In response to this northward (or non-southward) IMF, the plume began slowly rotating eastward and wrapping around the plasma-

sphere. In the 3:01 UT, 27 June EUV snapshot (panel (d)), the plume is approximately one MLT-hour eastward of its local time position at 14:06 UT, 26 June (panel (c)). LANL MPA data from 27 June are shown in Figure 10; L9 and L1 both saw evidence of plume rotation. In Figure 8(d) the gray orbit segment shows L9-observed plasmaspheric plasma whose location lines up with the EUV-observed plume, and is over 1 MLT-hour eastward of the plume location of Figure 8(b),(c). Hours later, during 10–12 UT, L4 measured plasmaspheric plasma between 17–19 MLT, supporting the plume rotation interpretation.

### 3.3. Flow at Geosynchronous Orbit

The sunward flows observed on 26 June 2000 by LANL MPA (satellites L9, L1 and L4) are plotted in Figure 11, in a format similar to that of Figure 5. The general features for this event are the same as found for the 2 June 2001 erosion: plume plasma on 26 June was observed to flow sunward, and flow speed fluctuations from this event seem to be related to fine-scale density structure (but as earlier, we note that these fluctuations may reflect measurement uncertainty as well). There is a general trend in the 26 June MPA flows for faster flow speeds to occur closer to dusk. In particular, the duskside, lower-density ( $< 30 \text{ cm}^{-3}$ ) portion of the plume seen by L4 was observed to be moving sunward at 10–30 km/s (corresponding to  $E \approx 1\text{--}3 \text{ mV/m}$ ) whereas the western portion (12–15 MLT) of the plume moved at speeds below 10 km/s ( $E < 1 \text{ mV/m}$ ). We speculate (as we did for the 2 June event) that the duskside flows may reflect SAPS activity; low-altitude DMS data do indeed contain evidence that SAPS flows were occurring after 5 UT on 26 June [Foster, private communication, 2003]. Particularly interesting is the separation of the plume into two distinct regions, a slowly-moving high density post-noon/pre-dusk region, and a much more rapidly-moving low density duskside region. Unfortunately, the evolution of the 26 June L4 dayside plume was not witnessed by EUV, but this ‘two-regime’ plume structure deserves more investigation in future work. MPA flow data from 27 June, plotted in Figure 12, show that the sunward flow speeds in the plume gradually decreased as the plume evolved. In Figure 12 the L9 density data shows the plume in the pre-dusk sector before 3 UT on 27 June; at this time the average sunward flow speed in the plume was about 5–6 km/s. Several hours later, L4 observed the rotating plume near dusk. Convection theory (presumably valid as long as SAPS flows are not present near dusk) predicts a flow stagnation point in the vicinity of dusk, and indeed the MPA-observed flows in the L4 duskside rotating plume were only of the order  $\sim 1 \text{ km/s}$  ( $E < 0.1 \text{ mV/m}$ ), and slightly antisunward in direction.

## 4. Conclusions

We used simultaneous global IMAGE EUV images and in situ LANL MPA density data together in two case studies of the formation and evolution of plasmaspheric plumes. The correspondence between EUV and MPA observations is extremely good; in each case study both local and global measurements showed the same location/shape and temporal behavior of the plume(s). This agreement helps validate the EUV image mapping process. We showed that not only do EUV and MPA agree, but the use of the two data sets provides a much more complete picture than either alone.

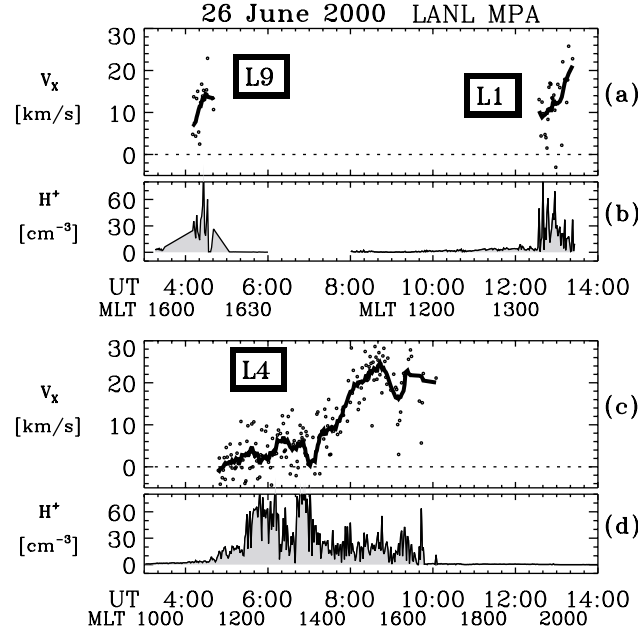


**Figure 11.** LANL MPA sunward flows of plume plasma, seen on 26 June 2000 during plasmasphere erosion. The format is similar to Figure 5, for LANL satellites L9, L1 and L4.

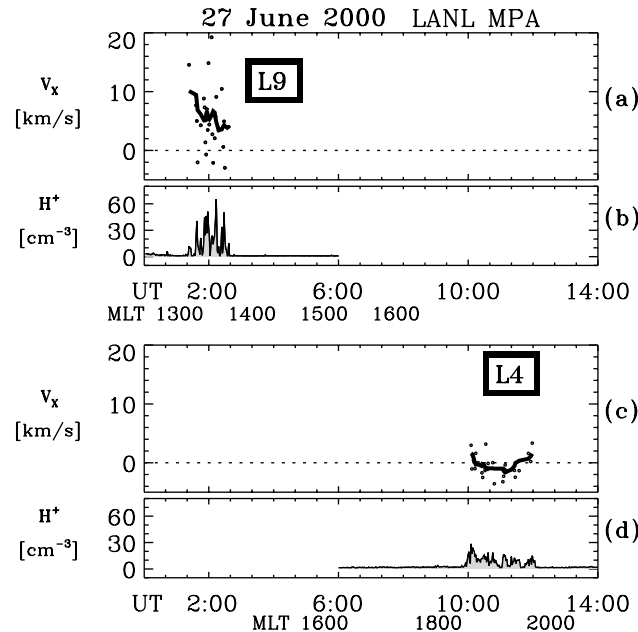


**Figure 12.** LANL MPA sunward flows of plume plasma, seen on 27 June 2000 during a quiet period in which the plume was rotating/wrapping. The format is similar to Figure 11, for LANL satellites L9 and L4.

The MPA instruments measure density far below the EUV threshold, and often see plasma outside the EUV field of view and/or at times when EUV is not well-positioned to image the plasmasphere. They also see much more of the plume's fine spatial structure, as shown in both events, but especially in the 26 June L4 (1994-084) data. The fine spatial structure inside plasmaspheric plumes hints at a very structured inner magnetospheric flow field, but may also be a remnant of structure in the quiet-time plasmasphere that is carried sunward during the erosion. EUV images provide a global view of plumes, permitting unambiguous separation of spatial and temporal effects in the MPA density profiles.

The plume's evolution follows the same pattern in both events (2 June 2001 and 26–27 June 2000). At the onset of erosion, the nightside plasmopause moves inward, creating a steep, well-defined density gradient that is relatively smooth in MLT. Dayside plasmaspheric plasma surges sunward and forms an initial dayside plume that is relatively wide in MLT. As the erosion continues over the course of hours, the plume's MLT extent becomes more narrow as the western plume edge rotates eastward, while the duskside edge remains roughly stationary for relatively steady solar wind conditions. Increases (decreases) in the solar wind speed and/or southward IMF strength cause the duskside plume edge to move westward (eastward). Ionosphere/ring-current coupling may also affect the duskside plume region. When the geomagnetic disturbance ends, the plume then begins to rotate with and/or wrap around the main plasmasphere, and flow speeds inside the plume slow down. This pattern of plume evolution was predicted by both theoretical and observational studies of plumes (e.g., *Grebowsky* [1970]; *Chen and Wolf* [1972]; *Spiro et al.* [1981]; *Elphic et al.* [1996]; *Weiss et al.* [1997]; *Lambour et al.* [1997]). The EUV images from our two case studies verify this plume evolution pattern.

Our study is distinguished from previous similar EUV/MPA comparisons [*Moldwin et al.*, 2003; *Spasojević et al.*, 2003b] in three ways. (1) Previous work compared MPA data with manually-extracted plasmopause curves; in our analysis we mapped the entire EUV image. The use of images allowed us to examine not only the location of the plume boundary, but the variation of density within the plume. (2) A mapped image from the 2 June 2001 event was crudely converted to a density distribution to demonstrate rough quantitative agreement between EUV and MPA number densities. This agreement demonstrates that it is in principle possible to produce reasonable number densities from EUV data, and points the way toward future studies that should include more extensive point-by-point comparisons between the two sets of observations. Most likely, work in this area will focus on quiet intervals in which there is a greater likelihood that dense plasma will be found at geosynchronous orbit. (3) We presented MPA-observed flow data that shows that plume plasma moves sunward, as expected from theoretical models (e.g., *Grebowsky* [1970]). We found some interesting flow properties that are worth further investigation. The sunward flow speeds weaken when the southward component of the IMF is reduced. The presence of the sub-auroral polarization stream (SAPS) may be involved in the tendency to find higher flow speeds near dusk, and may encourage the development of flow-shear instabilities in narrow, high-speed plasma channels. Indeed, the MPA measurements do suggest a link between sunward flow speed fluctuations and fine-scale density variations, suggesting that the inner magnetospheric E-field is highly structured. This possible link should be explored in future studies.

#### Acknowledgments.

We acknowledge N. Ness, C. Smith, D. McComas and the ACE science center for ACE MAG and ACE SWEPAM data. Work at Rice University (J.G. and P.H.R.) and Southwest Research Institute (J.G.) was supported by the IMAGE program under NASA contract NAS5-96020 and by the NASA SEC Guest Investigator program under NAG5-12787. Work at the University of Arizona (B.R.S.) was funded by subcontract with SwRI under NASA NAS5-96020. Work at the Los Alamos National Laboratory (M.F.T.) was conducted under the auspices of the U.S. Department of Energy. J.G. is grateful to Jim Burch for very helpful discussions. We thank both reviewers of this paper, whose comments were uniformly helpful.

#### References

- Borovsky, J. E., M. F. Thomsen, D. J. McComas, T. E. Cayton, and D. J. Knipp, Magnetospheric dynamics and mass flow during the November 1993 storm, *J. Geophys. Res.*, *103*, 26373, 1998.
- Burch, J. L., IMAGE mission overview, *Space Sci. Rev.*, *91*, 1, 2000.
- Burch, J. L., D. G. Mitchell, B. R. Sandel, P. C. Brandt, and M. Wüest, Global dynamics of the plasmasphere and ring current during magnetic storms, *Geophys. Res. Lett.*, *28*, 1159, 2001a.
- Burch, J. L., et al., Views of Earth's magnetosphere with the IMAGE satellite, *Science*, *291*, 619, 2001b.
- Carpenter, D. L., Relations between the dawn minimum in the equatorial radius of the plasmopause and Dst, Kp and the local K at Byrd Station, *J. Geophys. Res.*, *72*, 2969, 1967.
- Carpenter, D. L., and R. R. Anderson, An ISEE/Whistler model of equatorial electron density in the magnetosphere, *J. Geophys. Res.*, *97*, 1097, 1992.
- Carpenter, D. L., and J. Lemaire, Erosion and recovery of the plasmasphere in the plasmopause region, *Space Sci. Rev.*, *80*, 153, 1997.
- Chappell, C. R., K. K. Harris, and G. W. Sharp, A study of the influence of magnetic activity on the location of the plasmopause as measured by OGO5, *J. Geophys. Res.*, *75*, 50, 1970a.
- Chappell, C. R., K. K. Harris, and G. W. Sharp, The morphology of the bulge region of the plasmasphere, *J. Geophys. Res.*, *75*, 3848, 1970b.
- Chen, A. J., and R. A. Wolf, Effects on the plasmasphere of a time-varying convection electric field, *Planet. Space Sci.*, *20*, 483, 1972.
- Comfort, R. H., I. T. Newberry, and C. R. Chappell, Preliminary statistical survey of plasmaspheric ion properties from observations by DE 1/RIMS, in *Modeling Magnetospheric Plasma*, *Geophys. Monogr. Ser.*, edited by T. E. Moore and J. H. Waite Jr., vol. 44, p. 107, AGU, Washington, D. C., 1988.
- Craven, P. D., D. L. Gallagher, and R. H. Comfort, Relative concentration of He<sup>+</sup> in the inner magnetosphere as observed by the DE 1 retarding ion mass spectrometer, *J. Geophys. Res.*, *102*, 2279, 1997.
- Dent, Z. C., I. R. Mann, F. W. Menk, J. Goldstein, C. R. Wilford, M. A. Clilverd, and L. G. Ozeke, A coordinated ground-based and IMAGE satellite study of quiet-time plasmaspheric density profiles, *Geophys. Res. Lett.*, *30*(12), 1600, doi:10.1029/2003GL016946, 2003.
- Elphic, R. C., L. A. Weiss, M. F. Thomsen, D. J. McComas, and M. B. Moldwin, Evolution of plasmaspheric ions at geosynchronous orbit during times of high geomagnetic activity, *Geophys. Res. Lett.*, *23*, 2189, 1996.
- Foster, J. C., and W. J. Burke, SAPS: A new categorization for sub-auroral electric fields, *EOS Trans. AGU*, *83*, 393, 2002.
- Foster, J. C., P. J. Erickson, A. J. Coster, and J. Goldstein, Ionospheric signatures of plasmaspheric tails, *Geophys. Res. Lett.*, *29*(13), doi:10.1029/2002GL015067, 2002.
- Goldstein, J., R. W. Spiro, P. H. Reiff, R. A. Wolf, B. R. Sandel, J. W. Freeman, and R. L. Lambour, IMF-driven overshielding electric field and the origin of the plasmaspheric shoulder of May 24, 2000, *Geophys. Res. Lett.*, *29*(16), doi:10.1029/2001GL014534, 2002.

- Goldstein, J., B. R. Sandel, W. T. Forrester, and P. H. Reiff, IMF-driven plasmasphere erosion of 10 July 2000, *Geophys. Res. Lett.*, *30*(3), doi:10.1029/2002GL016478, 2003a.
- Goldstein, J., B. R. Sandel, and P. H. Reiff, Control of plasmaspheric dynamics by both convection and sub-auroral polarization stream, *Geophys. Res. Lett.*, *30*(24), 2243, doi:10.1029/2003GL018390, 2003b.
- Goldstein, J., M. Spasojević, P. H. Reiff, B. R. Sandel, W. T. Forrester, D. L. Gallagher, and B. W. Reinisch, Identifying the plasmopause in IMAGE EUV data using IMAGE RPI in situ steep density gradients, *J. Geophys. Res.*, *108*(A4), 1147, doi:10.1029/2002JA009475, 2003c.
- Grebowsky, J. M., Model study of plasmopause motion, *J. Geophys. Res.*, *75*, 4329, 1970.
- Horwitz, J. L., R. H. Comfort, and C. R. Chappell, A statistical characterization of plasmaspheric density structure and boundary locations, *J. Geophys. Res.*, *95*, 7937, 1990.
- Lambour, R. L., L. A. Weiss, R. C. Elphic, and M. F. Thomsen, Global modeling of the plasmasphere following storm sudden commencements, *J. Geophys. Res.*, *102*, 24351, 1997.
- McComas, D. J., S. J. Bame, B. L. Barraclough, J. R. Donart, R. C. Elphic, J. T. Gosling, M. B. Moldwin, K. R. Moore, and M. F. Thomsen, Magnetospheric Plasma Analyzer (MPA): Initial three-spacecraft observations from geosynchronous orbit, *J. Geophys. Res.*, *98*, 13453, 1993.
- McComas, D. J., S. J. Bame, P. Barker, W. C. Feldman, J. L. Phillips, P. Riley, and J. W. Griffiee, Solar wind electron proton alpha monitor (SWEPAM) for the Advanced Composition Explorer, *Space Sci. Rev.*, *86*, 563, 1998.
- Moldwin, M. B., M. F. Thomsen, S. J. Bame, D. McComas, and G. D. Reeves, The fine-scale structure of the outer plasmasphere, *J. Geophys. Res.*, *100*, 8021, 1995.
- Moldwin, M. B., B. R. Sandel, M. Thomsen, and R. Elphic, Quantifying global plasmaspheric images with in situ observations, *Space Sci. Rev.*, in press, 2003.
- Reinisch, B. W., et al., First results from the Radio Plasma Imager on IMAGE, *Geophys. Res. Lett.*, *28*, 1167, 2001.
- Roelof, E. C., and A. J. Skinner, Extraction of ion distributions from magnetospheric ENA and EUV images, *Space Sci. Rev.*, *91*, 437, 2000.
- Sandel, B. R., R. A. King, W. T. Forrester, D. L. Gallagher, A. L. Broadfoot, and C. C. Curtis, Initial results from the IMAGE extreme ultraviolet imager, *Geophys. Res. Lett.*, *28*, 1439, 2001.
- Sandel, B. R., J. Goldstein, D. L. Gallagher, and M. Spasojević, Extreme ultraviolet imager observations of the structure and dynamics of the plasmasphere, *Space Sci. Rev.*, in press, 2003.
- Smith, C. W., M. H. Acuna, L. F. Burlaga, J. L'Heureux, N. F. Ness, and J. Sheifele, The ACE magnetic field experiment, *Space Sci. Rev.*, *86*, 613, 1998.
- Spasojević, M., H. U. Frey, M. F. Thomsen, S. A. Fuselier, S. P. Gary, B. R. Sandel, and U. S. Inan, The link between a detached subauroral proton arc and a plasmaspheric plume, *Geophys. Res. Lett.*, in press, 2003a.
- Spasojević, M., J. Goldstein, D. L. Carpenter, U. S. Inan, B. R. Sandel, M. B. Moldwin, and B. W. Reinisch, Global response of the plasmasphere to a geomagnetic disturbance, *J. Geophys. Res.*, *108*(A9), 1340, doi:10.1029/2003JA009987, 2003b.
- Spiro, R. W., M. Harel, R. A. Wolf, and P. H. Reiff, Quantitative simulation of a magnetospheric substorm 3. Plasmaspheric electric fields and evolution of the plasmopause, *J. Geophys. Res.*, *86*, 2261, 1981.
- Su, Y.-J., M. F. Thomsen, J. E. Borovsky, and J. C. Foster, A linkage between polar patches and plasmaspheric drainage plumes, *Geophys. Res. Lett.*, *28*, 111, 2001.
- Thomsen, M. F., J. E. Borovsky, D. J. McComas, R. C. Elphic, and S. Maurice, The magnetospheric response to the cme passage of January 10-11, 1997, as seen at geosynchronous orbit, *Geophys. Res. Lett.*, *25*, 2545, 1998.
- Tobiska, W. K., T. Woods, F. Eparvier, R. Viereck, L. Floyd, D. Bouwer, G. Rottman, and O. R. White, The SOLAR2000 empirical solar irradiance model and forecast tool, *J. Atmos. Solar-Terr. Phys.*, *62*, 1233, 2000.
- Weiss, L. A., R. L. Lambour, R. C. Elphic, and M. F. Thomsen, Study of plasmaspheric evolution using geosynchronous observations and global modeling, *Geophys. Res. Lett.*, *24*, 599, 1997.
- Yahnin, A., et al., Features of steady magnetospheric convection, *J. Geophys. Res.*, *99*, 4039, 1994.

---

J. Goldstein, Space Science and Engineering Division, Southwest Research Institute, San Antonio, TX 78238 USA (jgoldstein@swri.edu)

B. R. Sandel, Lunar and Planetary Lab, University of Arizona, Tucson, AZ 85721 USA

M. F. Thomsen, Space and Atmospheric Sciences Group, Los Alamos National Laboratory, Los Alamos, NM 87545 USA

M. Spasojević, STAR Lab Packard Building, Stanford University, Stanford, CA 94305 USA

P. H. Reiff, Dept of Physics & Astron, Rice Univ, Houston, TX 77005 USA

(Received \_\_\_\_\_)